WPJET1-PR(17) 18560

A Drenik et al.

Automated detection and recognition of hot spots in protection video cameras at JET

Preprint of Paper to be submitted for publication in
Fusion Engineering and Design

This work has been carried out within the framework of the EUROfusion Consortium and has received funding from the Euratom research and training programme 2014-2018 under grant agreement No 633053. The views and opinions expressed herein do not necessarily reflect those of the European Commission.

Automated detection and recognition of hot spots in protection video cameras at JET

A. Drenik[1, 2], N. Osterman[2], P. Carvalho[3], G. F. Matthews[4], S. Brezinsek[5]

[1] Max-Planck-Institut für Plasmaphysik, Boltzmannstr. 2, 85748 Garching b. München, Germany,
[2] Jožef Stefan Institute, Jamova 39, SI-1000 Ljubljana, Slovenia,
[3] Instituto de Plasmas e Fusão Nuclear, IST, Av. Rovisco Pais, 1049-001 Lisboa, Portugal,
[4] Culham Centre for Fusion Energy, Abingdon, Oxon, OX14 3DB, United Kingdom,
[5] Forschungszentrum Jülich GmbH, Institut für Energie- und Klimaforschung – Plasmaphysik, Partner of the Trilateral Euregio Cluster (TEC), 52425 Jülich, Germany,
***** See the author list of "X. Litaudon *et al* 2017 *Nucl. Fusion* 57 102001"

Abstract

Hot spots on the divertor tiles at JET result in overestimation of the tile surface temperature which causes unnecessary termination of pulses. However, the appearance of hot spots can also indicate the condition of the divertor tile surfaces. To analyse the behaviour of the hot spots in the outer divertor tiles of JET, a simple image processing algorithm is developed. The algorithm isolates areas of bright pixels in the camera image and compares them to previously identified hot spots. The activity of the hot spots is then linked to values of other signals and parameters in the same time intervals. The operation of the detection algorithm was studied in a limited pulse range with high hot spot activity on the divertor tiles 5, 6 and 7. This allowed us to optimise the values of the controlling parametes. Then, the wider applicability of the method has been demonstrated by the analysis of the hot spot behaviour in a 3500-wide pulse range.

1. Introduction

JET is currently the largest operating tokamak, capable of running plasma pulses with a flat top duration of over 10 seconds and a routinely achievable combined heating power over 15 MW[1]. As a consequence, plasma wall interaction can, if uncontrolled, cause significant damage to the plasma facing components. This issue has become especially important after the installation of the ITER-like wall (ILW)[2], where the carbon-fibre composite (CFC) tiles in the divertor were replaced with bulk tungsten (W) and W-coated CFC tiles which impose stricter heat load restrictions. In order to prevent recrystallization of the bulk W tile, and the delamination of the W coatings, the surface temperature must be kept below 1200 °C[3,4]. To prevent such damage to the plasma facing components (PFCs) due to excessive heat loads, JET relies on an array of video cameras, *protection cameras*, which monitor the temperature of the plasma facing surfaces[5–7]. The field of view of each protection camera is split into regions of interest (ROIs). Each ROI provides a temperature signal, which represents the highest temperature (i.e. coming from the pixel with the highest intensity) within the ROI. A selected range of the temperature signals is included into the JET protection system. In the case that a temperature from an observed ROI exceeds the threshold value, defined by the plasma facing material of the ROI, for more than 0.4 seconds, a high temperature alarm is triggered and the pulse is stopped to prevent further damage to the plasma facing component[8]. The frequency of high temperature alarms, triggered by the signals from the protection cameras in a 3500 pulse-wide range from the start of the second ILW campaign is

plotted in Fig. 1 and it shows that the majority of the alarms are related to the high temperatures on three sections of the divertor: tile 5 (bulk W horizontal target) and tiles 6 and 7 (horizontal and vertical W-coated CFC targets in the outer divertor).

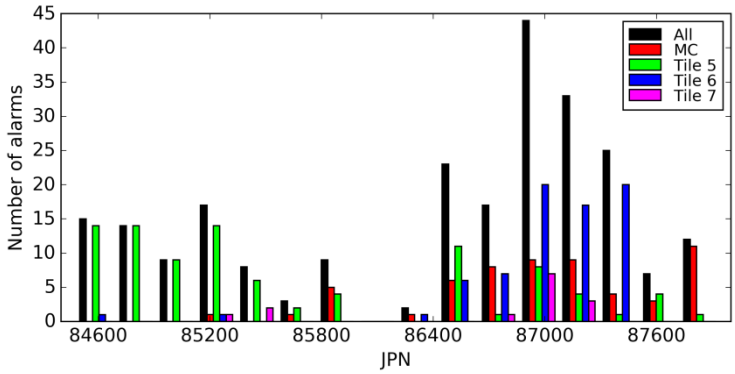

Figure 1. Frequency of high temperature alarms triggered by the protection cameras at JET, in a 3500-pulse long interval since the installation of the ILW

However, high temperature alarms are also triggered by hot spots – narrowly localized areas whose temperature is significantly higher than the underlying surface[5]. In such cases, the high value of the temperature signal does not represent the true temperature of the plasma component and the pulse is terminated on the basis of a false-positive alarm. On the other hand, the appearance of hot spots might also indicate accumulation of debris or molten material on the surface or delamination of the divertor tile coating. Material with poor adhesion to the surface can be mobilized which can lead to dust production and increased influx of impurities into the plasma[9]. It is thus in the interest of safe and efficient operation of a fusion device that the appearance and subsequent activity of the hot spots are well characterised. The temperature signals of the protection camera can provide some insight into the behaviour of the hot spots, however the low spatial resolution of the signals does not allow for a detailed analysis, nor are all of the areas of the viewing field of the cameras covered by the ROIs either. In this paper, we present a method of automated detection of the hot spots in the protection camera recordings, and the evaluation of their activity. The detection algorithm and the method of analysis of the hot spot activity are presented in the 2nd and 3rd section of the paper respectively and ultimately, the results of using the method on a demonstration pulse range are presented in the 4th section.

2. Detection and recognition of hot spots

The detection of hot spots is based on identifying isolated areas of bright pixels in the camera video feed, and comparing their size and location to the previously identified hot spots in the catalogue. The hot spot definitions are stored in the catalogue as lists of pixel which make up the isolated bright areas. The algorithm is described as follows:

1. In each frame, the image is binarised (i.e. pixels with a brightness above a certain `threshold` are set to 1, the others to 0).

2. Isolated areas of two or more bright pixels are indexed as lists of coordinates of the pixels they comprise.
3. Each area is compared against a catalogue of previously identified hot spots. If the area corresponds with a hot spot, the hot spot is labelled as active in the running frame number. Otherwise, the area is stored in a temporary catalogue of new hot spots.
4. After all frames in the video recording are processed, the temporary hot spots are filtered with the requirement of a minimum persistence over a certain number of frames (`min_persistence`). Those conforming to the requirement are added to the catalogue of verified hot spots. The periods of the activity of existing and newly added hot spots are filtered with the requirement of minimum duration of two consecutive frames.

The input data for the detection algorithm are raw video recordings. In case of the JET protection cameras, these are 288 pixel by 720 pixel monochrome videos with an 8 bit resolution, recorded at 49 frames per second. The pixel brightness, used in the detection algorithm, is the uncalibrated digital level of the video recording. This makes the analysis susceptible to variations of the camera sensitivity (e.g. due to gradual degradation of filters) and the pixel brightness is not directly related to the surface temperature. However, this way, the analysis can be performed on the entire viewing field of the camera and not just the calibrated areas. And thereby also avoiding uncertainties of calibration around the boundaries between different areas or reducing the spatial resolution as is the case in the temperature calculations.

The criteria used to check whether an isolated area of bright pixels corresponds to a previously identified hot spot are the following:

1. The area of the overlap between the bright pixel area and the hot spot must be greater than a certain fraction (`min_overlap`) of the surface area of the smallest of the hot spot or bright pixel area.
2. The surface area of the largest among the hot spot and the bright pixel area should not exceed the surface area of the smallest by a certain factor (`max_oversize`).

The operation of the algorithm is thus fully determined with four parameters: `threshold`, `min_persistence`, `min_overlap` and `max_oversize`.

The impact of these parameters was evaluated by processing the video recording from the KL1-P4DB camera, in a limited pulse range (ranges JPN 84758 – 84784 and 84955 – 84964, 87060 – 87095 and 87208 – 87240) in which high temperature alarms were being triggered with significant frequencies, by signals of that same camera, related to tiles 5, 6 and 7 respectively. The hot spot activity was analysed with `threshold` ranging from 80 to 254, and `min_persistence` ranging from 3 to 5. The parameters related to the recognition of existing hot spots were set for a relatively strict filter. The parameter `min_overlap` was set at 0.9 and `max_oversize` was set at 1.2.

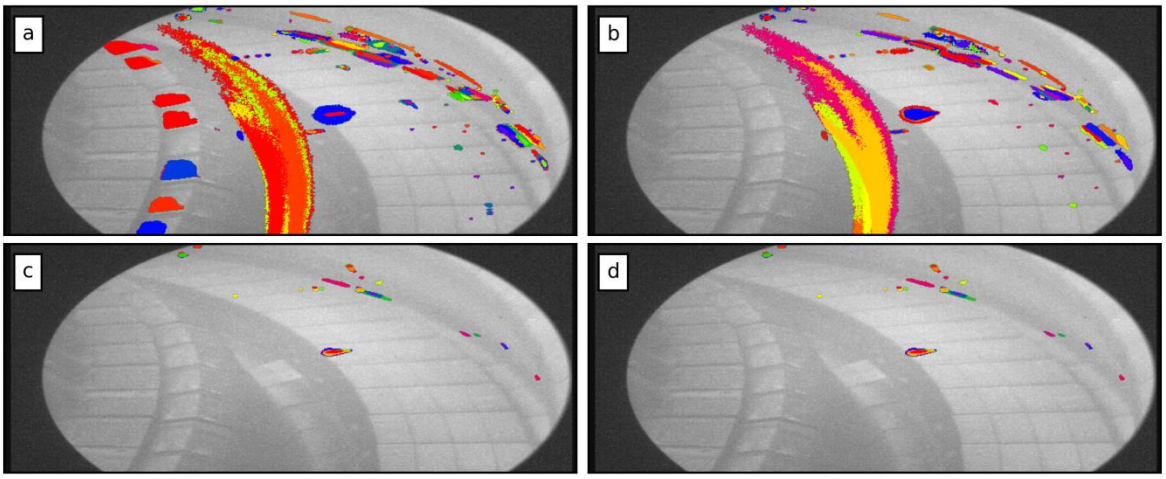

Figure 2. Catalogues of indexed hot spots at a: `min_persistence` = 3 and `threshold` = 80, b: `min_persistence` = 4 and `threshold` = 80, c: `min_persistence` = 4 and `threshold` = 220, d: `min_persistence` = 4 and `threshold` = 250

At low `threshold` values, the algorithm fails to distinguish between hot spots and non-hot spot features in the video images, such as the large, solid area inboard of tile 5, seen in Figs. 2a and b. The large areas most likely attain the necessary brightness during disruptions, MARFEs or reflections of the plasma radiation, bremsstrahlung, etc. from the neighbouring surfaces. This issue appears at all values of `min_persistence`, however is completely eliminated by raising `threshold` to 110 or 100 for `min_persistence` values of 3 and 4, and 5 respectively. At the lower `threshold` values, large solid areas on tile 4 are also indexed as hot spots (Fig. 2a), however only at values of for `min_persistence` 3. By applying increasingly stricter detection criteria (Figs a c and d), the number of detected hot spots is further reduced (Fig. 2c). The number of detected hot spots as a function of both parameters is shown in Fig. 3. The number of detected hot spots decreases throughout the range of `threshold` values, but does not vanish. Even at the threshold value which corresponds to the highest possible digital level value, a non-zero number of hot spots are detected at each value of `min_persistence`, as the activity of some hot spots results in the saturation of the camera image. It should be noted that, even at the strictest settings, certain features that are probably not linked to hot spots persist, most notably the elongated features along the edge of tile 6, whereas true hot spots are no longer detected (Fig. 2d).

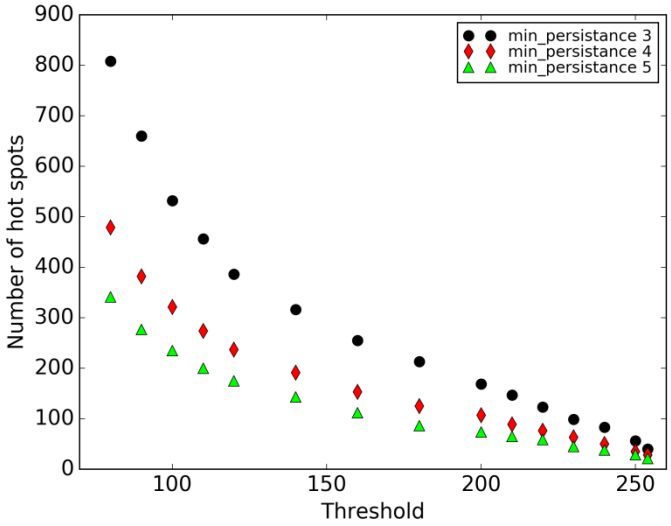

Figure 3. Number of detected hot spots versus the `threshold` value at different values `min_persistance`

The number of detected hot spots is also affected by the parameters which control the hot spot recognition criteria, `min_overlap` and `max_oversize`, i.e. the parameters which control the recognition of the existing hot spots. To evaluate the impact of the recognition criteria, the hot spot catalogues obtained at the strictest version of the filter were reprocessed with more relaxed recognition criteria, listed in Table 1. To estimate the overlapping hot spot definitions in the resulting catalogues, we observe the so-called average pixel coverage. This quantity is defined as the average number of hot spot definitions in the catalogue which include a particular pixel. For clarity, this statistic does not include the pixels which are not covered by any of the hot spot definitions in the catalogue. In the ideal case, when none of the hot spot definitions are overlapping, the average pixel coverage would thus be equal to 1, whereas higher values indicate overlapping hot spot definitions. A relatively large fraction of overlapping hot spots in the catalogue plots of Fig. 4 indicate that the correspondence criteria are indeed too stringent as the algorithm fails to recognize some of the hot spots. Then, the hot spot definitions are unnecessarily detailed and the same actual hot spot is covered by several catalogue entries, varying only little in size and position. With the most relaxed filter version, the average pixel coverage is reduced by approximately a factor of 3 compared to the most stringent version of the filter however the average pixel coverage is never exactly at 1, meaning that overlapping of hot spot definitions cannot be completely avoided. Moreover, when the criteria are too relaxed, however, several hot spots can be merged in a single, large area, which can also hinder the analysis of the hot spot activity. The optimal compromise between overly detailed definitions and over-merging was found to be at the filter version 3. The comparison between the detected hot spots with the strictest filter (version 0) and the chosen filter version 3 is also presented in Fig. 4, which shows a close up on a cluster of hot spots, as detected with both versions of the filter. With the stringent filter, the algorithm detects several hot spots of different sizes on the same part of the camera image whereas with the relaxed filter settings, the smaller hot spots are included in the definitions of the larger

ones with which they overlap. Accordingly, the number of detected hot spots in that area is reduced from 42 to 15.

Table 1: Filter settings used in analysis of the operation of the algorithm

Filter version	`min_overlap`	`max_oversize`
0	0.9	1.2
1	0.8	1.6
2	0.8	2.5
3	0.6	2.5
4	0.5	4

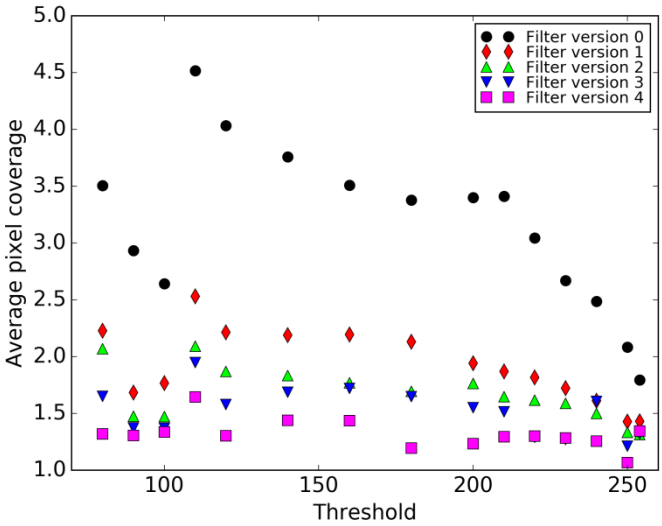

Figure 4. Average coverage of pixels by hot spot definitions, as a function of the `threshold` value, at the `min_persistence` value of 4. The break in the trend at `threshold` = 110 is due to the detection of large solid areas at lower threshold values, which distort the statistic by contributing a very large number of pixels.

Figure 5. Close up to a cluster of hot spots on tile 6 at filter version 0 (a) and the chosen filter version 3 (b), at the `threshold` of 180 and `min_persistance` at 4. With the version 0, the area is covered by 42 catalogue hot spot entries, while in the version 3 the number is reduced to 15.

3. Evaluation of the hot spot activity

For each individual hot spot, a database of several parameters is compiled by collecting the values of the parameter signals from intervals of its activity. In this particular analysis, the observed signals were the R and Z coordinate of the outer strike point and the total neutral beam injection (NBI) heating power. The complied database allows for the determination of the conditions which result in hot spot activity. For each parameter, the data points were plotted as 20-bin histograms. The central coordinate value was defined as the centre of the bin

with the highest count, while the lower and upper limits of the outer strike point coordinates were defined as the first bin respectively left and right of the central bin, which showed a count lower than 5 % of the maximum count. An example of the definition for the values of the R coordinate of the outer strike point (RSOL) for a hot spot located on tile 6 is shown in Fig. 6. In the case of NBI heating, only the lower limit was set. For each hot spot, these parameters then define the *activation area* for the outer strike point, and the minimum NBI power required to activate the hot spot.

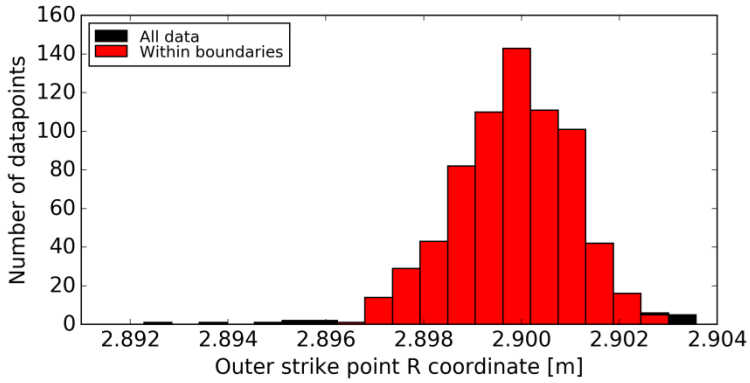

Figure 6. Definition of the RSOL boundary values for a hot spot on tile 6. The histogram shows all of the collected RSOL data, the red bars represent the data points within the defined boundary values.

The video recordings were processed in a sequence, starting from the earliest pulse in the range, using the same catalogue of hot spot definitions. In this test pulse range, the same catalogue was used also for processing with all of the `threshold` values, starting with the highest value. As increasing numbers of hot spots were detected at lower `threshold` values, they were added to the same catalogue, while keeping the definitions of the hot spots detected at higher values. This allowed for a study of the impact of the `threshold` value on the activation areas and minimum required NBI powers of individual hot spots.

The `threshold` value can have an impact on the position of the activation area of a hot spot, as is shown in Fig. 7. In a relatively narrow `threshold` range, the centre of the activation area shows a persistent trend of movement. This is likely caused by the fact that, at lower `threshold` values, less power is required for the luminosity of the hot spot in the camera image to reach (and exceed) the required value to register activity and therefore data points can be collected when the strike point is further away from the centre of the activation area than at higher `threshold` values. When the strike point, on average, spends more time on one side of the hot spot than on the other, the lowering of threshold will cause the activation area to shift towards the side on which the strike point spends more time. It should be noted, however, that the shift of the centre of the activation area is still smaller than its size. The impact of the `threshold` value on the required NBI power to activate the hot spots is also minimal. This is seen in Fig 8 which shows normed distribution of the number of hot spots per required minimum NBI power for five different `threshold` values. Excluding the bump in at around 3 MW, the low range of the distribution stops at 10 MW for the highest `threshold` values whereas it extends to lower powers for lower `threshold` values. Apart

from that, there is no discernible impact on the distribution. It should be noted, however, that in order to reduce the computation time, this analysis was performed on a limited number of pulses so the dataset does not cover a significant range of NBI powers. Unlike the strike point sweeps which provide continuous scan of the coordinates, the NBI heating is operated in a much more discrete fashion, i.e. mostly off or on at a set power. Thus, the analysed pulse range does not provide sufficient data to analyse the impact of the detection threshold on the required minimum NBI heating to trigger hot spot activity.

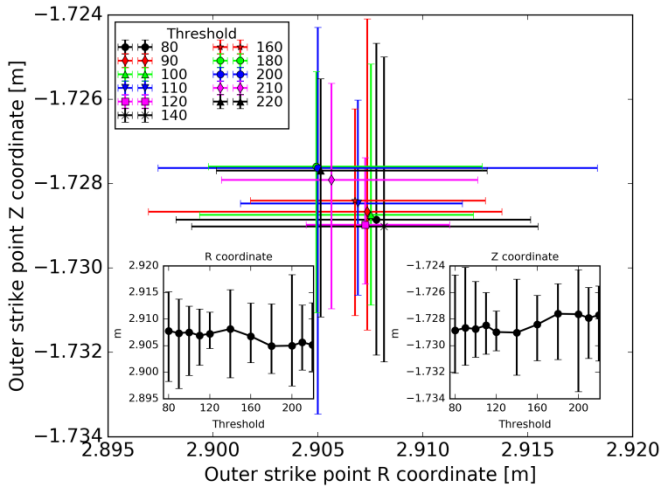

Figure 7. Impact of `threshold` on the identified strike point coordinates related to the activity of a hot spot.

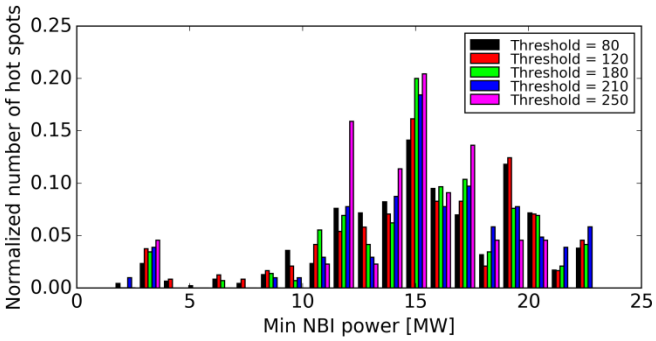

Figure 8. Impact of `threshold` on the identified minimum NBI heating, required for the activity of a hot spot.

4. Analysis of hot spot behaviour in the demonstration dataset

The appearance and activity of the outer divertor hot spots was analysed in a 3500-long pulse range starting at the second ILW campaign. The majority of the high temperature alarms (shown in Fig. 1) were triggered by signals representing the divertor tile temperatures. In the early pulses, the prevalent location of the alarms was the divertor tile 5, while later on, the frequency of alarms from tile 6 signals increased significantly, and the majority of the alarms were triggered by signals from the KL1-P4DB protection camera[5,7]. Due to the significant increase in the frequency of the alarms, the video recordings of this particular camera, in this

pulse range, was chosen as the dataset for the demonstration of the developed method of analysis.

To reduce the computing time, only the parts of the recordings during which the NBI heating power was above 2.5 MW were analysed as plasmas with lower heating powers were not expected to trigger hot spot activity. This reduced the number of analysed video recordings to a total of 1749, with the average running time of 14.1 s per pulse. The video analysis was performed at the `min_peristance` value of 4, the recognition filter version 3, and the `threshold` values of 180, 200, 210, 220, 230, 240 and 250. The catalogue images are shown in Fig. 9, for some of the `threshold` values. As expected from the algorithm benchmarking, even at the lowest `threshold` value, the catalogue does not contain any obvious non-hot spot features or large illuminated areas. However, certain features in the images can be attributed to features which exhibit hot spot like temperature behaviour, but are not *de facto* hot spots. These are the Langmuir probe tips, seen along a straight line across tile 5, and the exposed tungsten lamella on the inboard side of tile 5, which was deliberately melted in a dedicated experiment[10,11]. The number of detected Langmuir probe tips is reduced considerably at the highest `threshold` value, but the exposed lamella persists all throughout the range. At lower values, other non-hot spot features include the elongated areas along tile 6. The number thereof, too, is reduced by raising the `threshold` value, however, they are not completely eliminated. It can be also noted that, apart from the deliberately exposed surfaces, very little hot spots were detected on the surface of tile 5, which is not surprising as the surfaces of bulk-W tiles are expected to be more resilient than W-coating on CFC tiles, and for geometrical reasons, accumulation of debris is not expected to be the most prominent in this part of the divertor[12].

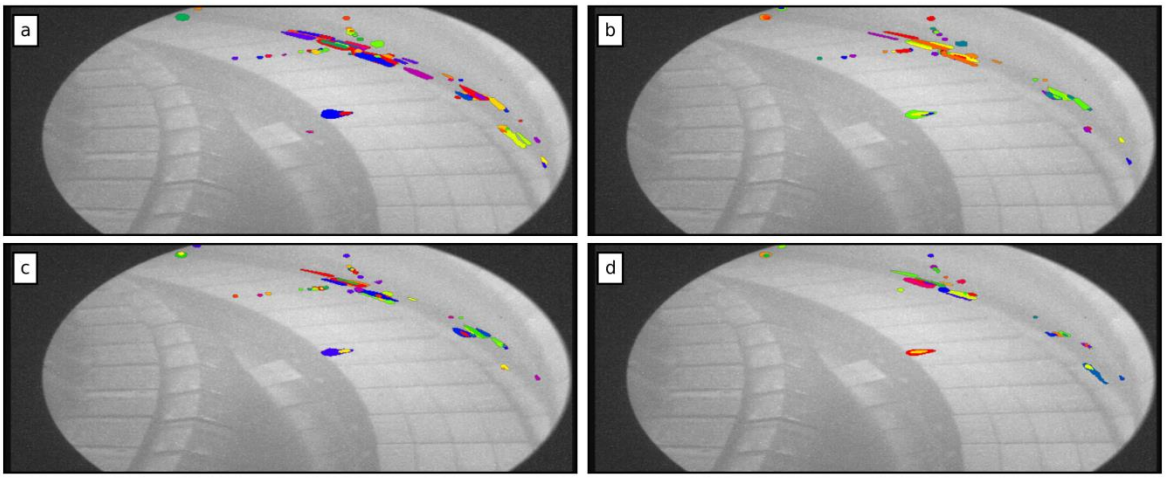

Figure 9. Catalogue images of hot spots detected in the demonstration pulse range, for `threshold` values 180 (a), 210 (b), 230 (c) and 250 (d)

For each `threshold` value, the analysis was performed twice in a row with the same catalogue of identified hot spots. This way, the hot spots were identified and added to the

catalogue only in the first run, whereas in the second run, all of the hot spots that would appear throughout the pulse range were already included at the beginning of the analysis. Fig. 10 shows histograms of first appearance of the hot spots in the first and second run, at `threshold` values 180, 210, 230 and 250. First appearance denotes the first pulse number in the pulse range at which the algorithm registers activity for a particular hot spot. While the appearance of hot spots is spread out over the whole pulse range, at each `threshold` value, the first observed activity in the second run tends to gravitate towards lower pulse numbers, compared to the first one. In order to register activity of an existing hot spot, the required persistence is only 2 consecutive frames in the video recording, opposed to the 4 required to register a new hot spot in the catalogue. Accordingly, 2nd run thus provides more accurate information about the hot spot activity, so the results discussed in the remainder of the text are going to be obtained from the 2nd runs.

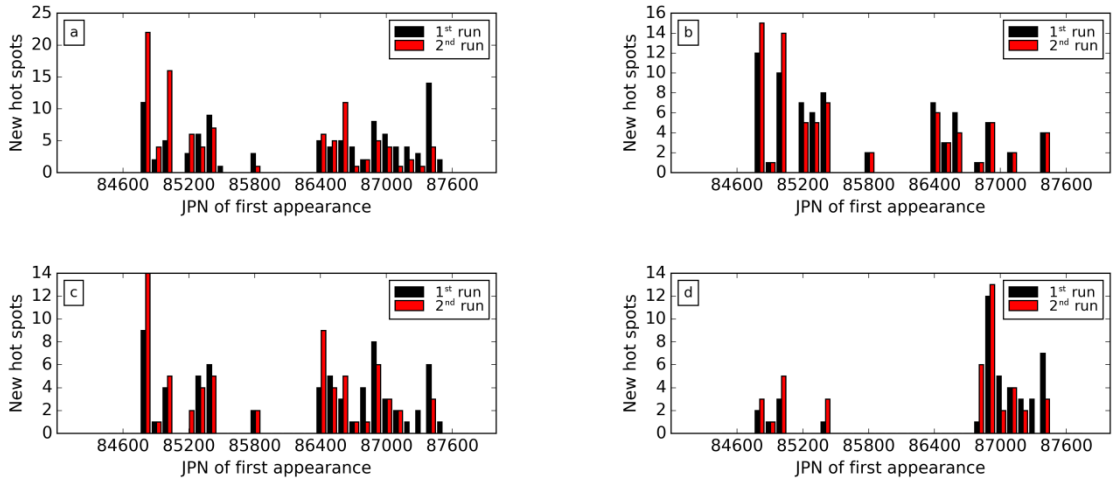

Figure 10. First noted hot spot activity in the first and second run, for `threshold` values 180 (a), 210 (b), 230 (c) and 250 (d)

The first appearance of hot spots grouped by their location (divertor tile 5, 6, or 7) is shown in Fig. 11, for `threshold` values 180, 210, 230 and 250. The locations of the hot spots are determined from the identified central position of the activation area. There are two intervals of particular activity, roughly between JPNs 84800 and 85500, and later between JPNs 86400 and 87500. This is in agreement with the frequency of the high temperature alarms (Fig. 1). The distribution of the hot spot appearance by divertor tiles, too, agrees with the alarms in Fig. 1, as in the first interval, most of the hot spots appear on tile 5, whereas in the second they appear on tiles 6 and 7. It should be noted that, at all threshold values, the hot spots on tile 5 are detected in the beginning of the pulse range. This would suggest that such hot spots are present on the surface of tile 5 since the beginning of the pulse range and show activity as soon as the conditions are met. It is also noteworthy that at the highest `threshold` setting, the number of hot spots detected on tile 5 drops considerably, which is very much in line with the observation from the catalogue images in Fig 9.

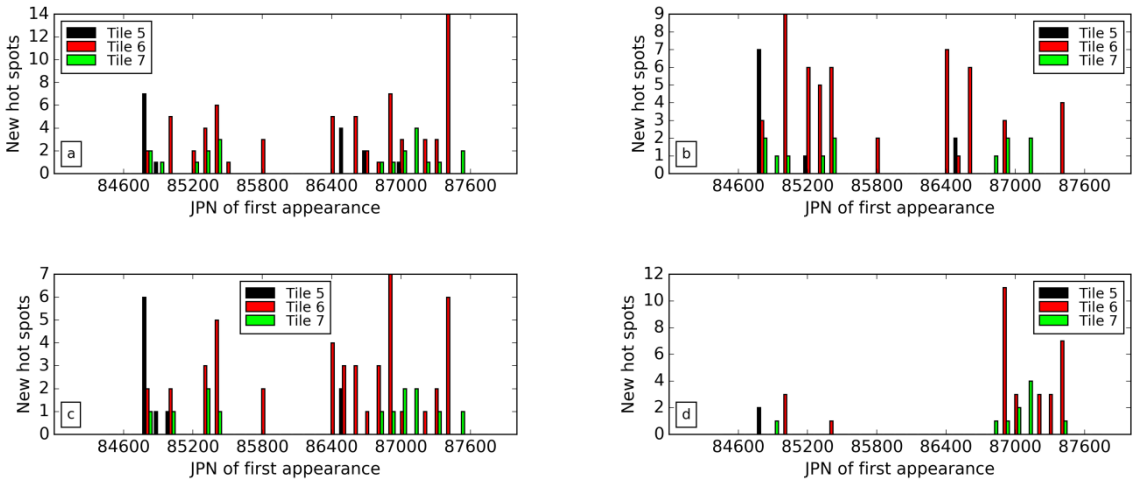

Figure 11. First noted hot spot activity in second run shown for each tile, for `threshold` values 180 (a), 210 (b), 230 (c) and 250 (d)

Similar observations are presented in Fig. 12, which plots the fraction of the hot spots that have been detected up to a certain pulse, for each tile and several values of `threshold`. In line with Figs 11 and 9, the majority of the hot spots on tile 5 are detected very early in the pulse range. At the highest threshold settings, Fig. 9 shows the only detected hot spots on tile 5 are related to the W-melt experiments. Accordingly, Fig. 12 shows that all of the tile 5 hot spots are detected during the pulses performed within this experiment. At lower threshold values, the majority of the hot spots is still detected at the same pulse numbers, however the trend is distorted by the detection of additional hot spot like features (e.g. Langmuir probe tips) later in the range, at around JPN 86520. The detection of hot spots on tiles 6 and 7 is spread more evenly throughout the pulse range, however only for `threshold` values below 250. At the highest setting, the shape of detection is profoundly different. The majority of the hot spots are detected between pulse numbers 86800 and 87100. As the analysis is done with uncalibrated data, the discrepancy among the trends at lower and the highest threshold value could be related to sudden changes in the camera sensitivity. However, the detection of hot spots at the highest threshold setting coincides with the increased frequency of high temperature alarms from tiles 6 and 7. The alarms are triggered by calibrated temperatures, thus the detected behavior is also likely to be related to an increase of the hot spot activity on the surfaces of tiles 6 and 7.

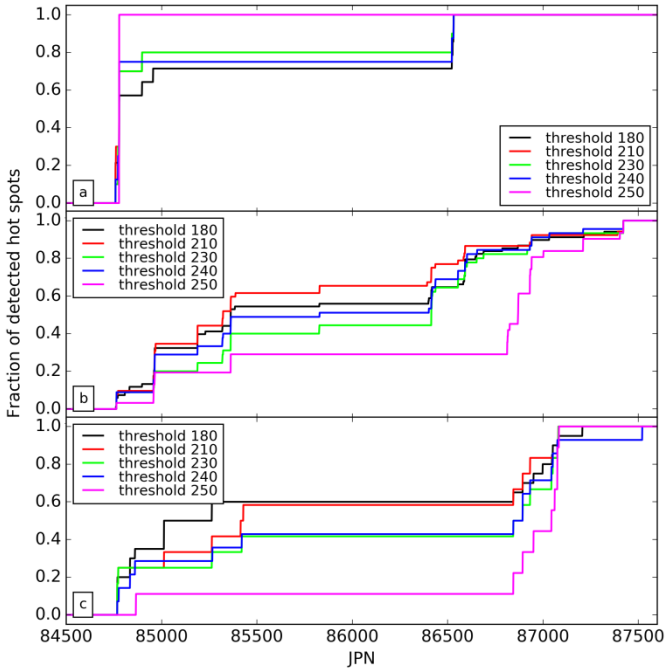

Figure 12. Fraction of detected hot spots (from the total catalogue entries) on tiles 5 (a), 6 (b) and 7 (c), for different `threshold` values

As outlined in the previous section, the collected data of the outer strike point coordinates and the NBI heating power from the intervals of hot spot activity define the activation areas and minimum NBI power for each hot spot. Based on this, it is possible to analyse and track the activity of the hot spots throughout the pulse range, in relation to the position of the outer strike point and the NBI heating power. In each pulse we observe:

- *good time*: total time in which the outer strike point was within the defined activation areas, and the NBI heating power was above the minimum value,
- *hot time*: the time of hot spot activity within the good time intervals (with a minimum duration of two consecutive video frames).

The combined good and hot times are shown for the hot spots on tiles 6 and 7, detected at `threshold` value of 250 are shown in Figs 13a and 13b respectively. The quantities are combined for all hot spots which appear before and after JPN 86000, i.e. hot spots detected before the main appearance on the two tiles, as shown in Figs 12b and 12c. Throughout the pulse range, the good time of both groups is remarkably similar, both in terms of absolute values as well as the trends. The hot time trends are less similar as the first group shows a higher amount of activity. Besides the first part of the pulse range, where by definition, only the first group will show activity (non-zero hot time values), it is more active in the majority of the pulse range. However, this statistic can be easily distorted by the fact that some of the hot spots in the camera image are included in the ROIs which provide signals for the high temperature alarms, while others are not. This means that the activity in some hot spots triggers an alarm and terminate the pulse (thereby limiting its activity), whereas in others, it doesn't, and they are therefore allowed to shine for considerably longer time per pulse.

Between pulse numbers 86300 and 86800, relatively high amounts of good time per pulse are recorded, however the algorithm doesn't detect any activity in the hot spots. It should also be noted that between JPNs 87000 and 87200, there is distinctively higher activity in the hot spots which are detected after JPN 86000. In this case, this corresponds to the difference in the good time between each group.

These results clearly show that the conditions for activity of the both groups are met with the approximately same frequency throughout the pulse range, based on the observed parameters, which could thus show that the detected hot spots are created in changes on the surface of the divertor tiles. However, it could also suggest that additional parameter should be included in the analysis, or that at this `threshold` setting, the algorithm fails to detect activity in the hot spots in a significant fraction of the pulse range.

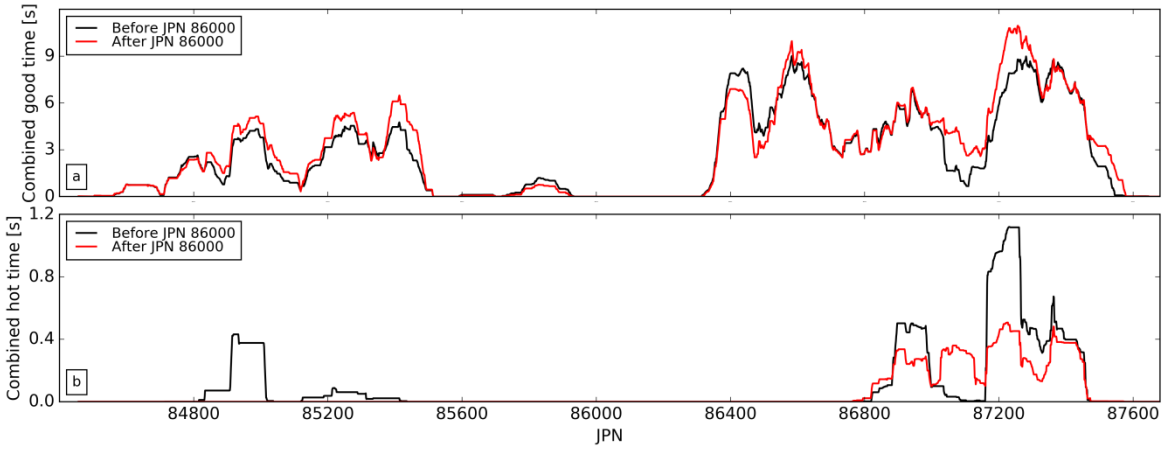

Figure 13. Rolling average (50-pulse wide) of the combined good time (a) and hot time (b), per pulse, for hot spots on divertor tiles 6 and 7 which appear before and after JPN 86000, detected at the `threshold` value of 250

A stronger correlation between good time and hot time is observed at the lowest `threshold` value (180), seen in Fig. 14. In this case, the pulse number that separates the two groups of hot spots is moved to JPN 85200, as this is the point before the biggest jump in the fraction of detected hot spots on both tiles (Fig. 12). However, the main features of the results obtained with the highest `threshold` setting are obtained at the lowest, as well. Namely, conditions for activity of the hot spots detected after JPN 85200 are met with similar frequency before and after they show their first activity, and in the pulses between JPNs 87000 and 87200, they exhibit distinctly different trends of activity than the hot spots detected before JPN 85200. The fact that these features are evidently independent of the `threshold` setting increases our confidence in the interpretation that the hot spots observed on tiles 6 and 7 indeed occur due to changes on the surfaces of the tiles. More than that, it shows that these changes are more likely to be gradual than abrupt. The hot spots first start to appear shortly after JPN 85200, however only after JPN 86800 their luminosity increases to the point that they are detected at the highest `threshold` setting (reflected also in the frequency of the high temperature alarms).

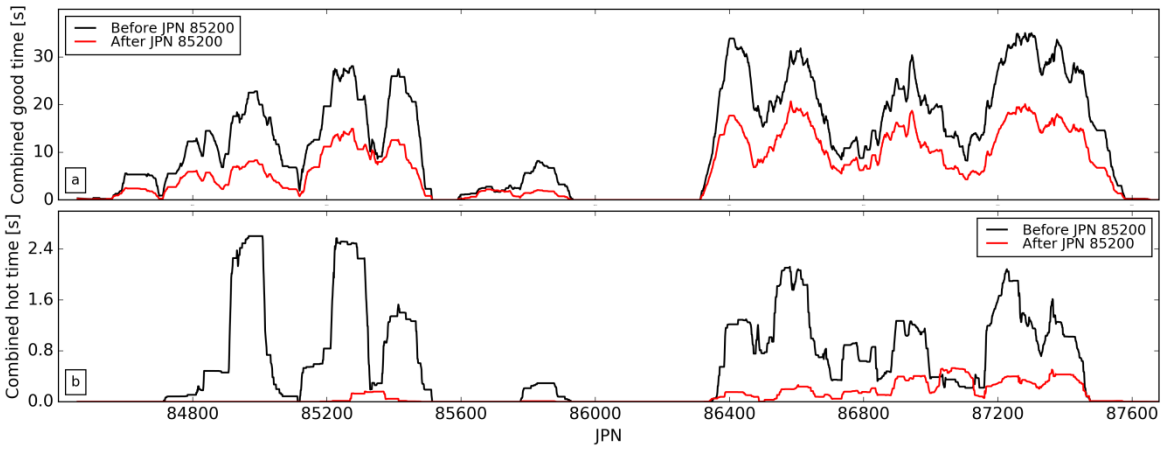

Figure 14. Rolling average (50-pulse wide) of the combined good time (a) and hot time (b) for hot spots on divertor tiles 6 and 7 which appear before and after JPN 82000, detected at the `threshold` value of 180

The activation areas of the majority of the hot spots on tiles 6 and 7 are smaller than 5 cm, as seen in Fig. 15. At lower `threshold` values, the distribution is extended to a small number of hot spots with a larger activation size (8 cm), however apart from that, the `threshold` setting does not seem to have a detectable impact on the distribution of the activation areas.

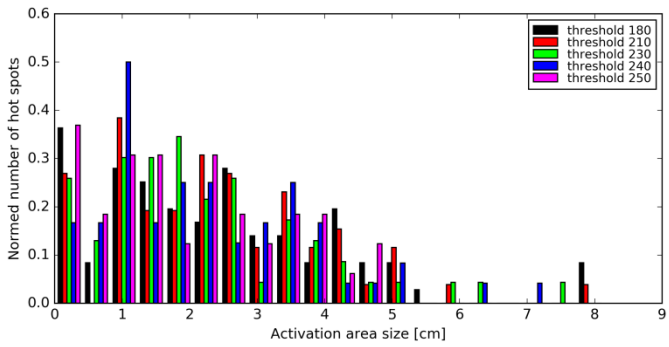

Figure 15. Normed distribution of the size of collection areas of hot spots on tiles 6 and 7 at the `threshold` values of 180, 210, 230, 240 and 250 (b)

5. Conclusions

To gain insight into the behaviour of hot spots on the divertor tiles of JET, a method of automated hot spot detection, recognition and analysis was developed. The method comprises two parts: an image analysis algorithm which provides the detection of individual hot spots in the recordings of protection cameras and the evaluation of their activity, and statistical analysis which links the identified hot spot activity to values of other parameters and signals.

In this particular case, the hot spot activity was compared to the coordinates of the outer strike point and the NBI heating power.

The input for the hot spot detection and recognition algorithm are raw video recordings. While this means that the activity of the hot spots is not accurately related to the calibrated surface temperature, it also means that the algorithm does not rely on pre-processed signals. The analysis can therefore be performed on the complete field of view of the camera and the spatial resolution of the detection is limited only by the camera's properties.

The operation of the image analysis algorithm is fully controlled by four parameters. Two of them control the detection of hot areas in the analysed images, while the other two control the recognition of the detected hot areas as previously identified hot spots. The impact of the parameters was observed on the hot spot detection in a limited pulse range. The findings of the brief analysis allowed to identify the set of parameters which ensures reliable detection and recognition of hot spots on the divertor surfaces, without influences of noise or events of sudden increased image brightness such as disruptions. The impact of the image binarisation threshold could also be, to an extent, detected in the identified boundaries of the outer strike point coordinates which corresponded to the activity of the hot spot.

The method of analysis was demonstrated on video recordings from a camera focused on the outer divertor, in a 3500 pulse wide range. The observed appearance and activity of the hot spots in general agrees with the frequency of the high temperature alarms triggered by the protection system. Based on the results of the detection algorithm, the activity of the hot spots was analysed in relation to the coordinates of the outer strike point and the NBI heating power. This analysis demonstrated that unlike the deliberately exposed areas on tile 5 (bulk W), the majority of the hot spots on tiles 6 and 7 (W-coated CFC) appeared as consequences of gradual changes on the surfaces of the tiles. The results then show that the hot spots with a low intensity of activity can be used as an early warning signal of changes on the divertor tiles before they start causing the observed high temperature alarms. Linking the appearance of the hot spots to their causes in the operation history of JET falls outside of the scope of this paper. It is, however, the belief of the authors that the presented method of analysis of the hot spot behaviour, together with the algorithm of automated hot spot detection and recognition, and evaluation of their activity, will serve as an important tool in future analysis of the condition of divertor tiles, and the events linked to it. Beside the analysis of the behaviour of hot spots from past campaigns, analysis of the data from a running campaign will help to identify potential hot spots before they evolve to the point of prematurely terminating pulses by causing high temperature alarms, while the identified plasma parameter values will serve as input data for shaping future discharges to avoid further degradation of the divertor surfaces.

6. Acknowledgements

This work has been carried out within the framework of the EUROfusion Consortium and has received funding from the Euratom research and training programme 2014-2018 under grant agreement No 633053. The views and opinions expressed herein do not necessarily reflect those of the European Commission.

7. References

[1] F. Romanelli, M. Abhangi, P. Abreu, M. Aftanas, J.E.T. Contributors, et al., Overview of the JET results, Nucl. FUSION. 55 (2015). doi:10.1088/0029-5515/55/10/104001.

[2] V. Riccardo, M. Firdaouss, E. Joffrin, G. Matthews, P. Mertens, V. Thompson, E. Villedieu, Operational limits for the ITER-like wall in JET, Phys. Scr. T138 (2009). doi:10.1088/0031-8949/2009/T138/014033.

[3] H. Maier, R. Neu, H. Greuner, B. Boeswirth, M. Balden, S. Lindig, G.F. Matthews, M. Rasinski, P. Wienhold, A. Wiltner, Qualification of tungsten coatings on plasma-facing components for JET, Phys. Scr. T138 (2009). doi:10.1088/0031-8949/2009/T138/014031.

[4] P. Mertens, V. Philipps, G. Pintsuk, V. Riccardo, U. Samm, V. Thompson, I. Uytdenhouwen, Clamping of solid tungsten components for the bulk W divertor row in JET-precautionary design for a brittle material, Phys. Scr. T138 (2009). doi:10.1088/0031-8949/2009/T138/014032.

[5] G. Arnoux, S. Devaux, D. Alves, I. Balboa, C. Balorin, N. Balshaw, M. Beldishevski, P. Carvalho, M. Clever, S. Cramp, J.-L. de Pablos, E. de la Cal, D. Falie, P. Garcia-Sanchez, R. Felton, V. Gervaise, A. Goodyear, A. Horton, S. Jachmich, A. Huber, M. Jouve, D. Kinna, U. Kruezi, A. Manzanares, V. Martin, P. McCullen, V. Moncada, K. Obrejan, K. Patel, P.J. Lomas, A. Neto, F. Rimini, C. Ruset, B. Schweer, G. Sergienko, B. Sieglin, A. Soleto, M. Stamp, A. Stephen, P.D. Thomas, D.F. Valcarcel, J. Williams, J. Wilson, K.-D. Zastrow, J.-E. Contributors, A protection system for the JET ITER-like wall based on imaging diagnostics, Rev. Sci. Instrum. 83 (2012). doi:10.1063/1.4738742.

[6] V. Huber, A. Huber, D. Kinna, I. Balboa, S. Collins, N. Conway, P. Drewelow, C.F. Maggi, G.F. Matthews, A.G. Meigs, P. Mertens, M. Price, G. Sergienko, S. Silburn, A. Wynn, K.-D. Zastrow, In-vessel calibration of the imaging diagnostics for the real-time protection of the JET ITER-like wall, Rev. Sci. Instrum. 87 (2016). doi:10.1063/1.4959912.

[7] A. Huber, D. Kinna, V. Huber, G. Arnoux, I. Balboa, C. Balorin, P. Carman, P. Carvalho, S. Collins, N. Conway, P. McCullen, S. Jachmich, M. Jouve, C. Linsmeier, B. Lomanowski, P.J. Lomas, C.G. Lowry, C.F. Maggi, G.F. Matthews, T. May-Smith, A. Meigs, P. Mertens, I. Nunes, M. Price, P. Puglia, V. Riccardo, F.G. Rimini, G. Sergienko, M. Tsalas, K.-D. Zastrow, J.E.T. Contributors, The near infrared imaging system for the real-time protection of the JET ITER-like wall, Phys. Scr. T170 (2017). doi:10.1088/1402-4896/aa8a14.

[8] D.F. Valcarcel, D. Alves, P. Card, B.B. Carvalho, S. Devaux, R. Felton, A. Goodyear, P.J. Lomas, F. Maviglia, P. McCullen, C. Reux, F. Rimini, A. Stephen, L. Zabeo, K.-D. Zastrow, J.E. Contributors, The JET real-time plasma-wall load monitoring system, FUSION Eng. Des. 89 (2014) 243–258. doi:10.1016/j.fusengdes.2013.10.010.

[9] V. Rohde, M. Balden, T. Lunt, A.U. Team, Dust investigations at ASDEX Upgrade, Phys. Scr. T138 (2009). doi:10.1088/0031-8949/2009/T138/014024.

[10] J.W. Coenen, G. Arnoux, B. Bazylev, G.F. Matthews, S. Jachmich, I. Balboa, M. Clever, R. Dejarnac, I. Coffey, Y. Corre, S. Devaux, L. Frassinetti, E. Gauthier, J. Horacek, M. Knaup, M. Komm, K. Krieger, S. Marsen, A. Meigs, P. Mertens, R.A. Pitts, T. Puetterich, M. Rack, M. Stamp, G. Sergienko, P. Tamain, V. Thompson, J.-E. Contributors, ELM induced tungsten melting and its impact on tokamak operation, J. Nucl. Mater. 463 (2015) 78–84. doi:10.1016/j.jnucmat.2014.08.062.

[11] G.F. Matthews, B. Bazylev, A. Baron-Wiechec, J. Coenen, K. Heinola, V. Kiptily, H. Maier, C. Reux, V. Riccardo, F. Rimini, G. Sergienko, V. Thompson, A. Widdowson,

J.E.T. Contributors, Melt damage to the JET ITER-like Wall and divertor, Phys. Scr. T167 (2016). doi:10.1088/0031-8949/T167/1/014070.
[12] A. Baron-Wiechec, E. Fortuna-Zalesna, J. Grzonka, M. Rubel, A. Widdowson, C. Ayres, J.P. Coad, C. Hardie, K. Heinola, G.F. Matthews, J. Contributors, First dust study in JET with the ITER-like wall: sampling, analysis and classification, Nucl. FUSION. 55 (2015). doi:10.1088/0029-5515/55/11/113033.